Investigation into paraffin wax and ethylene vinyl acetate blends for use as a carrier vehicle in ceramic injection moulding

Standring, Tom; Blackburn, Stuart; Wilson, Paul

DOI:
10.1080/03602559.2015.1132434

Document Version
Peer reviewed version

Citation for published version (Harvard):
Standring, T, Blackburn, S & Wilson, P (ed.) 2016, 'Investigation into paraffin wax and ethylene vinyl acetate blends for use as a carrier vehicle in ceramic injection moulding', *Polymer - Plastics Technology and Engineering*. https://doi.org/10.1080/03602559.2015.1132434

INVESTIGATION INTO PARAFFIN WAX AND ETHYLENE VINYL ACETATE BLENDS FOR USE AS A CARRIER VEHICLE IN CERAMIC INJECTION MOULDING

T. Standring[a], P. Wilson[b], S. Blackburn[a]
a. Chemical Engineering, University of Birmingham, Edgbaston, UK, B15 2TT.
b. Rolls-Royce plc, Derby, UK, DE24 9HY.

Abstract

An experimental study into paraffin wax (PW) and ethylene vinyl acetate (EVA-28) blends has been undertaken to investigate the potential for their use as carrier vehicles for ceramic injection moulding applications. Carrier systems are critical for the fabrication of this type of moulded component; making their properties at all stages of the process of great importance.

Blend formulation was performed on a modified planetary mixer, with materials testing and characterisation being conducted through thermogravimetric analysis, differential scanning calorimetry, rheometry and mechanical testing. Crystallisation was captured using a hot stage optical microscope.

PW and EVA-28, in most circumstances, combine to form stable homogeneous blends, which experience relatively small changes in the melting and solidification phase transition behaviour. However, these blends exhibit notable viscosity shifts and flexural strength performance changes with increasing EVA-28 content.

The melt flow behaviour of the blends at shear rates of 100 s^{-1} varies from 0.01 Pa.s for PW to 10 Pa.s for the composition by weight of 50 % PW and 50 % EVA-28, which literature suggests is the upper limit of viscosities for successful carrier systems. All PW/EVA-28 blends experience shear thinning behaviour with increasing shear rate, which can be modelled with reasonable accuracy using the Cross and Carreau models. Increasing the EVA-28 content in a blend causes the initiation of shear thinning at progressively lower shear rates and also forms a blend with an increasing elastic character at typical injection temperature. Yield stress is not developed for blends containing less than fifty weight percent EVA-28.

The addition of EVA-28 significantly alters the mechanical properties of the blends, modifying the brittle nature of PW to develop increasing flexible and plastic properties. Although with less than twenty-five weight percent EVA-28 in a blend fracture failure still results, greater EVA-28 content represses the failure mechanisms developing increasing degrees of plastic deformation.

1. Introduction

Ceramic Injection Moulding (CIM) is a common method for the mass fabrication of high precision net-shape ceramic components, the process is facilitated through a carrier vehicle imparting adequate flow properties to the ceramic powder to enable filling of a die. The carrier vehicle is also required to maintain the integrity of the moulded shape until a point in firing where the ceramic can achieve this role unaided (1).

Often the main differences in CIM systems are directly related to the carrier system, highlighting its importance in the process (2). Key properties of a successful carrier vehicle include; compatibility of the blended binder materials, flow characteristics and the ability to impart desired mechanical strength whilst the moulded component is in the green state. Once mixed with ceramic, the carrier system must exhibit good wetting behaviour and advantageous interactions with the ceramic powder. An efficient de-bonding programme is finally required to remove the carrier vehicle from the component prior to the sintering stage (1;3).

It is preferable to produce the simplest carrier system due to the manufacturing, storage and economic benefits. However, as the area of study is sometimes considered more of an art than a science it is not uncommon to find, as stated by Blackburn and Wilson, that some paste or dough systems used in industry evolve into complex mixtures (4). Some of these can contain over 10 components due to practitioners 'tweaking' the formulations to overcome processing issues as and when they appear, rather than developing a comprehensive understanding.

Paraffin wax (PW) is a common major binder found in carrier vehicles for CIM, due to it possessing high fluidity once molten, low molecular weight, relatively low shrinkage (typically less than 10 %) and non-reactive with the systems (1;5-17). Minor binders are used to modify the major binder properties and assist in the debind process by making it more progressive than sudden. Ethylene vinyl acetate (EVA) is a material which has been used to achieve an increase in strength properties of solidified blends and thus the moulded components (1;9;12;15;18).

The interactions between PW and EVA have been investigated to a limited degree in the literature, and a number of these works, such as those covering the oil industry, have investigated the behaviours in a solution rather than a melt (19;20). Of those involved with CIM applications, the EVA co-polymer investigated contained low vinyl acetate additions and was aimed at high pressure injection moulding. To the authors knowledge a full characterisation across the composition range in these blends is not available in the literature (1;9;21).

This paper reports a comprehensive characterisation of a range of properties within formulated blends of PW and EVA with a high vinyl acetate content, and address the implications of these properties to CIM. In particular this paper focuses upon the important

properties of thermal and flow behaviour along with flexural strength. Flow characterisation included the effects of temperature and shear as well as the viscoelastic behaviour of the blends.

2. Experimental Procedures

2.1 Materials

Blends were formed from paraffin wax (Sasolwax) and ethylene vinyl acetate (DuPont, ELVAX), with Figure 1 displaying the representative structure for each material. EVA is a co-polymer of ethylene and vinyl acetate, with the material investigated containing 28 weight percent vinyl acetate. Increasing the poly(vinyl acetate) segments (q in Figure 1) in an EVA co-polymer causes a reduction in the crystallinity with a completely amorphous and rubber-like EVA expected when the vinyl acetate content is greater than 43 weight percent (22). Both materials have a low thermal conductivity with PW and EVA having values of around 0.2 $W.m^{-1}.K^{-1}$ (23), and 0.311-0.34 $W.m^{-1}.K^{-1}$ (24) respectively. However, in the blended feedstock, the much higher relative thermal conductivity of the ceramic, often in the region of 1.5 to 10 $W.m^{-1}.K^{-1}$ will dominate (25;26).

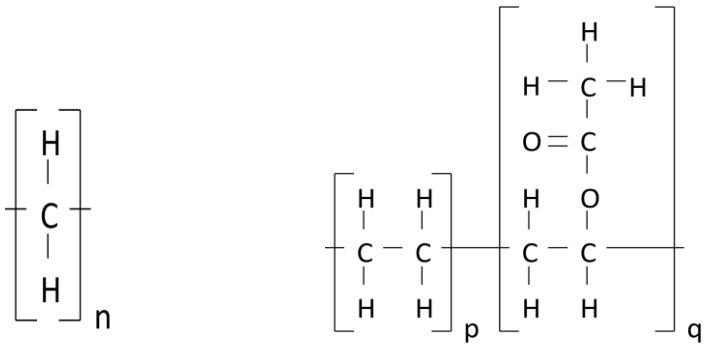

Figure 1: Schematic for PW (left) and EVA (right) structures. PW has the chemical formula of C_nH_{2n+2}; were n is between 20 and 40. For EVA; p is semi-crystalline polyethylene with values between 500 and 5,000 and q is an amorphous vinyl acetate co-polymer.

2.2 Equipment

2.21 Thermogravimetric Analysis (TGA)

Thermogravimetric analysis (TGA) conducted on a Mettler Toledo instrument was used to determine the degradation temperature profiles of the materials. Temperature was increased at a rate of 10 $^{o}C{\cdot}min^{-1}$ in the temperature range of 25 to 600 ^{o}C. Samples were weighed to 0.1 mg precision with a typical sample mass of 40 mg.

2.22 Blending: Planetary Mixer

Blends were prepared in a modified Metcalfe planetary mixer, at 125 ^{o}C, utilising a beater mixing attachment. The blends were mixed under low shear for 1 hour. Mixing temperature and time was chosen to ensure melting of all components but low enough to prevent degradation of the materials as predetermined by the TGA. PW was added first to the mixer with the EVA included once the PW was fully molten. Formulated blends were poured into moulds of rectangular shape (90 x 9 x 9 mm) for storage prior to use in feedstock manufacture and to allow for later mechanical testing.

2.23 Differential Scanning Calorimetry (DSC)

Thermal analysis was conducted on a 'Mettler Toledo 5433' differential scanning calorimeter under nitrogen flow. The instrument was calibrated with high purity metal standards (indium) to ensure accuracy of the temperature scale. Samples (5-10 mg weighed to 0.1 mg precision) were heated from -20 to 150 ^{o}C and held at temperature for 3 minutes (heating cycle 1). The temperature was then reduced to -20 ^{o}C before re-heating the sample to 600 ^{o}C (heating cycle 2), with all ramps conducted at a rate of 10 ^{o}C·min^{-1}. The cyclic heating was used in order to remove any thermal effects and/or eliminate pan filling differences. To eliminate these effects the blend melting data was taken from the second heating cycle whereas crystallisation data was found to be independent of cycle number. DSC analysis allowed for determination of phase transitions, as well as the enthalpy of fusion and crystallisation. Repeats were completed to verify data.

2.24 Hot Stage Optical Microscopy (HSOM)

Image capture of the blends was conducted using HSOM. The apparatus comprised an Olympus B-509 microscope and a Linkam hot stage, allowing a maximum temperature of 600 ^{o}C to be reached. Samples were placed on a glass plate and heated to 120 ^{o}C, on cooling at a rate of 1 ^{o}C·min^{-1} the solidification process was captured using the Linkam software. The images were taken in cross-polarised light which allowed the onset of crystal development to be captured more precisely (light crystals in a dark field).

2.25 Rheometry

Rheometry was conducted on a Malvern Gemini HR Nano controlled stress rheometer. The temperature effects on viscosity were determined using a 40 mm parallel plate and constant shear rate of 100 s^{-1}, allowing a direct comparison with literature data describing carrier systems used in CIM applications, with a 150 µm gap between the plates (2). Samples were cooled from a temperature of 95 ^{o}C at a rate of 10 ^{o}C·min^{-1}. The effect of shear between 0.1 and 10,000 s^{-1} was conducted at 80 ^{o}C using the same geometry and gap size (blends were initially melted at 95 ^{o}C).

Yield stress measurements were conducted at 80 ^{o}C, using the same parallel plate but with a 500 µm gap, by observing the instantaneous viscosity behaviour with small changes in shear stress (up to 100 Pa), to determine initial resistance to flow.

Dynamic rheological measurements were carried out to determine the congealing point of each blend, parallel plate geometry incorporating a 20 mm plate and a 500 µm gap was used. The congealing point was determined by conducting temperature sweeps in the pre-determined linear viscoelastic region (LVR). The LVR denotes the region in which the storage modulus (G') remains constant for a material subjected to a fixed frequency (1 Hz) and stepwise increases in the amplitude of the applied stress. Above a critical stress, G' begins to decrease and this region of non-linear dependence results in the mathematical equations applied not being appropriate to describe the material behaviour.

Repeats were conducted on all rheological measurements, however, in some cases only a representative test run has been displayed.

2.26 Mechanical Testing

Mechanical testing was conducted on a Lloyd Instruments load frame. Testing was conducted in a water bath set to 25 ^{o}C for ten minutes. A three-point bend test was used for testing using a span of 65 mm and cross head speed of 10 mm·min^{-1}. The blends were moulded into test bar geometries of dimensions 90 x 9 x 9 mm. Due to apparatus limitations, the maximum flexural strain which could be imparted on the carrier vehicle blends was 0.2.

Blends with an EVA content of greater than sixty weight percent were unable to be moulded successfully due to their high apparent viscosity.

Flexural testing enables the flexural modulus, flexural strength (commonly referred to as modulus of rupture, MoR) and energy to fracture to be determined. The flexural modulus (Equation 1) is defined as the gradient of the flexural stress (Equation 2) vs flexural strain (Equation 3) graph taken from the initial linear portion up to 0.01 strain. The flexural strength (Equation 4) is described by the load at fracture. The energy of fracture is described by the area encompassed under the flexural stress vs flexural strain graph up to the point of fracture failure.

Flexural Modulus (MPa), $$\sigma_m = \frac{P.L^3}{4.w.h^3.D} \quad (1)$$

Flexural stress (MPa), $$\sigma_f = \frac{3.P.L}{2.w.h^2} \quad (2)$$

Flexural strain (-) $$\epsilon_f = \frac{6.D.h}{L^2} \quad (3)$$

Flexural strength (MPa), $$\sigma_{Max} = \frac{3.L.P_{FRACTURE}}{2.w.h^2} \quad (4)$$

P is the load at a given point on the load-deflection curve (N), L is support span (mm), w is width of test geometry (mm), h is thickness of test geometry (mm) and D is deflection at centre of test geometry (mm).

3. Results and Discussion

3.1 Blend Formulation

PW/EVA blends were formed by varying the EVA content between 0 and 100 weight percent, between 0 and 30 % the EVA was varied in 5 % additions and from 30 to 100 % the EVA was increased in 10 % addition increments. The thermal decomposition behaviours of the primary materials (PW and EVA) between 25 and 600 ^{o}C is given in Figure 2 and shows that no material degradation occurred at the blending temperature of 125 ^{o}C. PW begins to decompose at approximately 200 ^{o}C, with EVA beginning to decompose at 300 ^{o}C. Both materials are shown to have fully decomposed by 600 ^{o}C.

PW decomposes continually between 200 ^{o}C and 400 ^{o}C which is due to its differing chain lengths. EVA undergoes initial loss of acetic acid at around 350 ^{o}C, followed by thermal scission of the backbone methylenic chain, beginning around 450 ^{o}C and so has two distinct removal stages (27-29).

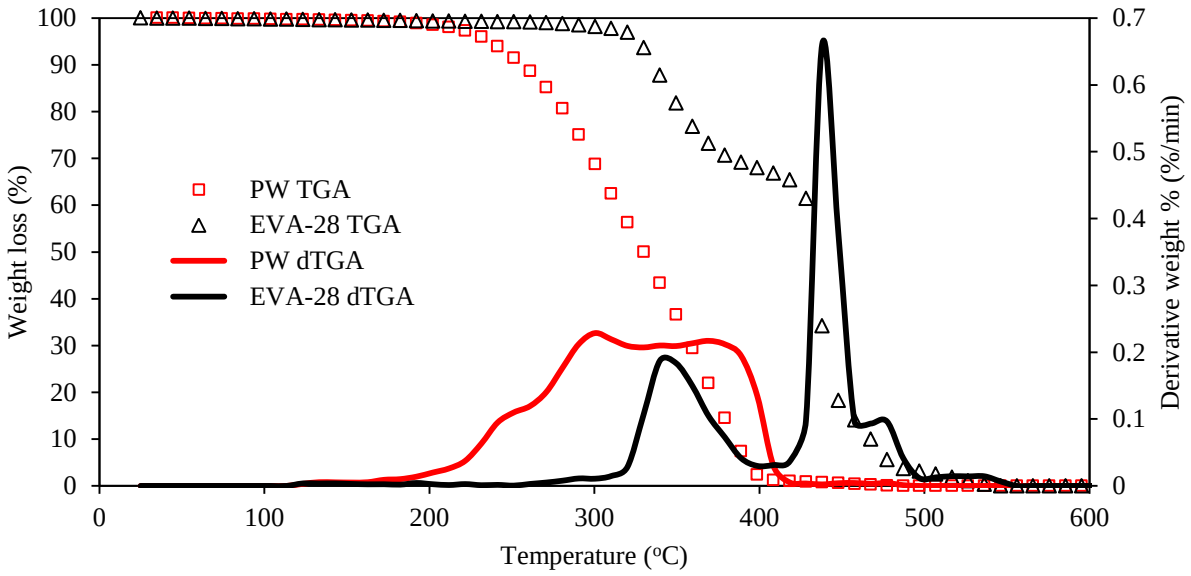

Figure 2: TGA and dTGA of PW and EVA (25 ^{o}C to 600 ^{o}C at 10 ^{o}C·min^{-1}).

3.2 Upper Processing Temperature

The melting point of each blend, as determined by DSC, offers valuable information into the required processing conditions for CIM. The thermal profile for PW contains two distinct peaks (Figure 3) with the initial small peak maximum at approximately 43 ^{o}C due to solid-solid transitions, and the larger peak with a maximum at around 60 ^{o}C describing the main melting peak. Complete melting of all crystalline material occurs at around 68 ^{o}C but this is not easily observed on the figure due to the shallow gradient of the trace line near to this temperature.

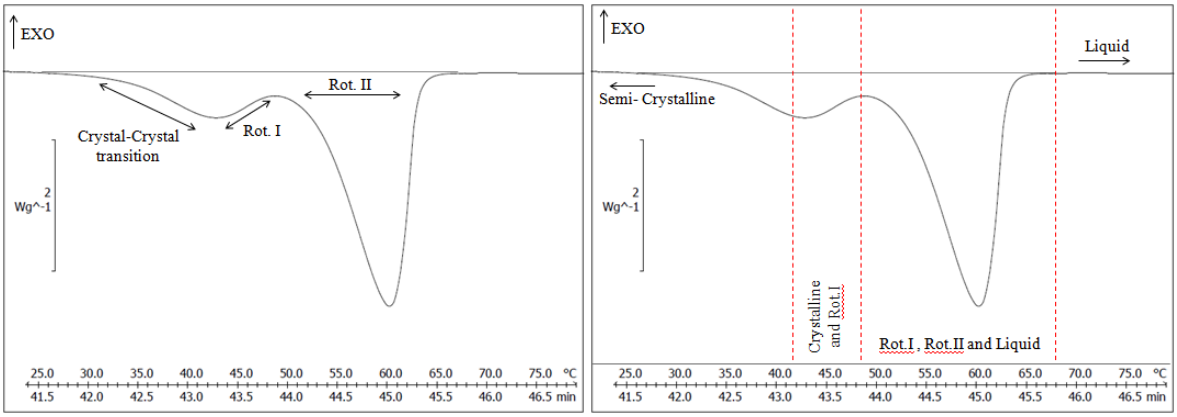

Figure 3: DSC heating trace of paraffin wax (heating rate of 10 ^{o}C·min^{-1}) describing transitions (left) and state of material (right) with increasing temperature.

The low temperature peak is associated with the solid-solid phase transition between the crystalline phases and then transition into the pre-melting mesophase of the wax, rotator phase 1 (Rot. I) (30;31). Below this temperature there is a fully crystalline state, were crystalline forms can be monoclinic (even n-alkanes with n > 26), triclinic (even alkanes with n < 26) or orthorhombic (odd n-alkanes) (20;32;33). However, in mixtures an orthorhombic crystal structure is known to occur even if the pure components exhibit different structures (34).

With further heating of PW a larger peak is observed, this describes the transition from the Rot. I phase to differing rotator phases before reaching a liquid form, the point where the trace line rejoins the baseline. Rotator phases are made up of lamellar crystals but differ from the low-temperature crystalline phase due to the degree of rotational freedom they possess around their long axis (35). There are five known rotator phases which differ by the form of the thermal motion around their long axes (36;37). Normal alkanes typically possess several different rotator phases over a short temperature span prior to melting and so only remain in one particular phase for a few degrees which makes some rotator phases difficult to observe (38), for this reason only the Rot. II is highlighted on Figure 3. Complete transition of all present mesophases to the isotropic liquid phase occurs around 68 ^{o}C. It has been proposed that the solid-solid transition is a good estimate of the solidus and the main melting peak corresponds to the liquidus (39).

PW exhibits a broad melting peak area, describing the enthalpy of fusion, due to the variations in its chain length causing the formation of crystal elements of slightly different sizes and types, with these requiring different values of energy to melt. Overall the PW analysed absorbs 200 $J.g^{-1}$ in transition from its ordered crystal phase to its disordered liquid phase (calculated from integration of the area under the DSC trace relative to a user determined baseline, defined as an endotherm) equating to about 80 % total crystallinity when comparing against literature values for 'pure' (100 % crystalline) PW (quoted as 253.7 $J{\cdot}g^{-1}$) (40). This value is consistent with figures from the literature (41).

EVA-28, due to its low levels of crystallinity, absorbs 20 $J{\cdot}g^{-1}$ during melting as can be seen in the DSC trace shown in Figure 4. Previous research suggests that polyethylene converts from the crystalline phases to the Rot. III phase before entering the isotropic liquid phase with further heating, however, in the co-polymer the melting point of the crystal elements is lower than expected for polyethylene and instead appears to coincide with Rot. II phase formation (40).

Like PW, EVA also melts over a broad region with onset of melting occurring at about 42 ^{o}C, peak melting of crystalline elements was observed at 62 ^{o}C and the materials crystallinity completely melted around 84 ^{o}C. EVA contains two glass transition temperatures, one from both polyethylene and polyvinyl acetate. Polyethylene has a glass transition in the region of -30 ^{o}C, however, due to the cooling limitations of the DSC the entire transition could not be observed. Polyvinyl acetate has a glass transition in the range of 25 to 39 ^{o}C which is highlighted by the small peak before the melting peak in the DSC trace (42).

If literature guidelines are followed where the poly(vinyl acetate) segments are assumed to be non-crystalline and the enthalpy of fusion of the pure polyethylene segments are taken as 277.1 $J{\cdot}g^{-1}$ then crystallinity in the EVA-28 is 7.9 %, which is also consistent to the crystallinity found in the literature for EVA with 28 weight percent vinyl acetate (22;43).

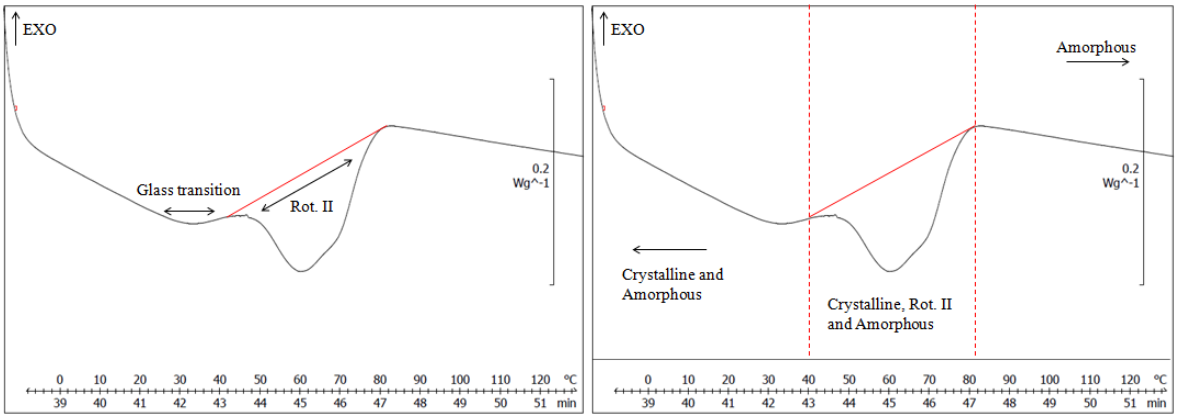

Figure 4: DSC heating trace of EVA (heating rate of 10 $^{o}C{\cdot}min^{-1}$) describing transitions (left) and state of material (right) with increasing temperature.

The heating profiles of PW and EVA show markedly different thermal behaviours, as displayed in the bottom and top DSC traces in Figure 5 respectively, which is a direct result of the differing levels of crystallinity in their structures. Due to the normalised nature of the DSC traces, the EVA trace appears as only a very marginal deviation from the baseline. The endothermic profiles displayed by the DSC analysis describe the crystal elements of each blend absorbing energy in order to undertake transitions or melting. The DSC traces illustrate predominantly crystalline features of the materials, however, each blend is semi-crystalline and amorphous when solid but after complete melting each blend is purely amorphous. Closer inspection of two blends possessing 30 and 70 % EVA are displayed in Figure 6, with proposed transitions clearly labelled for reference. Interpretation of the phase behaviour of blends using exclusively DSC curves is difficult due to the potential overlap in peaks, and subsequent difficulty in identifying the transition forms.

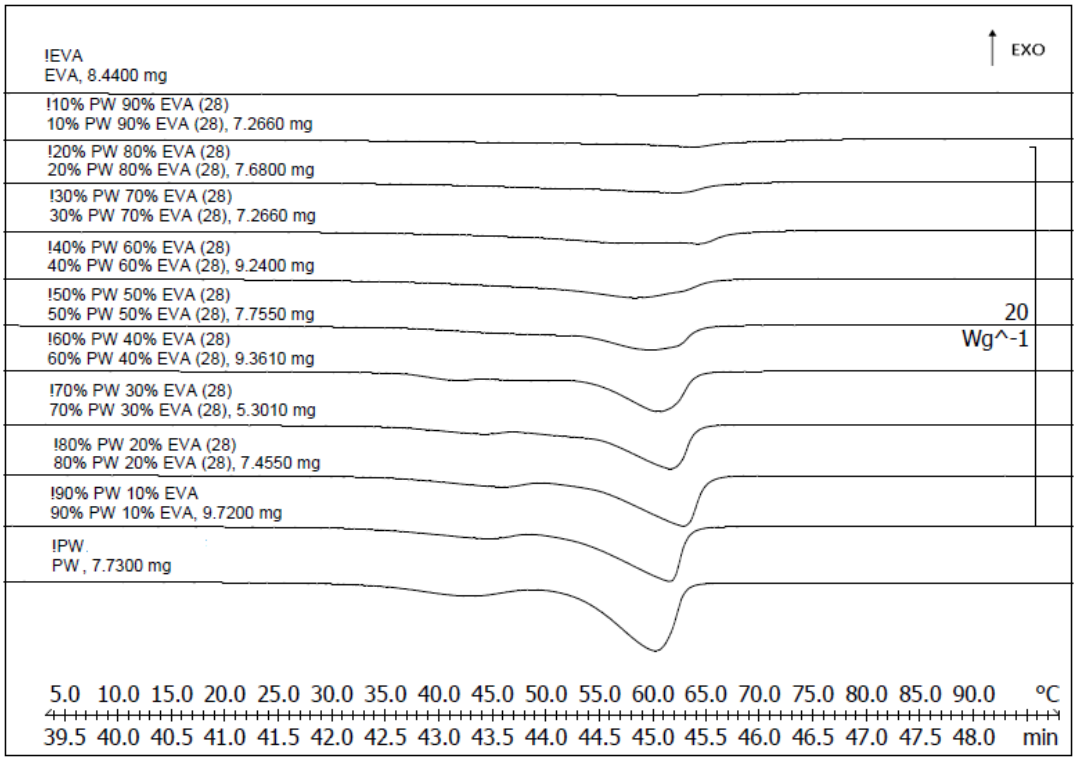

Figure 5: DSC analysis of paraffin wax and ethylene vinyl acetate blend (data from heating cycle 2, -20 ^{o}C to 600 ^{o}C at a rate of 10 $^{o}C{\cdot}min^{-1}$).

Increasing the EVA-28 content in PW/EVA blends has a significant effect on the DSC melting profile; as shown in Figure 5. A general feature is observed of both shallower and broader peaks describing the increased range of melting points in the blends. The solid-solid transition peak, a feature from PW in the blends, decreases in magnitude as the EVA content increases. However, the transition is eliminated at around 40 weight percent EVA and is attributed to the developed structure retarding the process. The melting peak area also decreases in magnitude with increasing EVA reflecting the reduction in PW content. The traces for blends formed using low concentrations of EVA, typically less than about 30 %, are shown to be highly influenced by paraffin wax, however, as EVA-28 has similar melting

characteristics to PW at this concentration its presence is additionally not distinguishable on the traces. When high concentrations of EVA are added to PW there are more noticeable thermal effects, and it is clear at 70 weight percent additions of EVA the solid-solid crystal transition occurring in PW is suppressed, Figure 6. At this concentration of EVA two apexes on the main melting peak are seen suggesting a slight phase separated structure, however, this phenomena only occurred in the 70:30 blend suggesting it only takes place in a small composition range.

The transition points from the DSC analysis are plotted in Figure 7, to make the effects of EVA additions more clearly distinguished. The plotted figures describe the solid-solid transition (described by temperatures below the dotted line and depicted as region A in Figure 6) and broad rotator phase regions (region B in Figure 6) with the dotted line illustrating, for reference, the peak melting point in the blends.

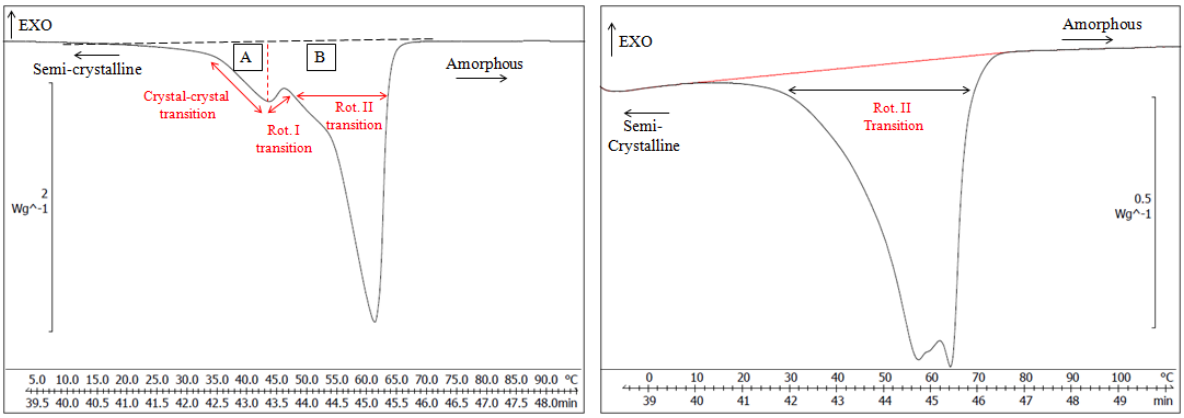

Figure 6: DSC traces highlighting heating profile 2 for 70 % PW 30 % EVA (left) and 30 % PW 70 % EVA (right) (heating rate of 10 $^{o}C\,min^{-1}$).

3.3 Injection Temperature

The feedstock (ceramic and carrier system mix) should be introduced into the die as close to the so-called 'congealing point' temperature as possible to minimise the amount of cooling required for the carrier vehicle to set, for waxes this region is where the crystalline material establishes a spanning network (44). Oscillatory rheometry enables the congealing point to be determined but it requires initial determination of the linear viscoelastic region (LVR). The LVR for PW/EVA blends is highlighted in Figure 8, the LVR holds up to when the storage modulus decreases which signifies a break down in the blend structure. During testing it was not possible to measure the LVR for blends with less than thirty weight percent EVA and blends with thirty to forty weight percent EVA have only debatable linear regions, highlighting their unstable and weak structures. PW was too unstable to gather appropriate data. An increased level of EVA-28 forms blends which exhibit greater elastic character.

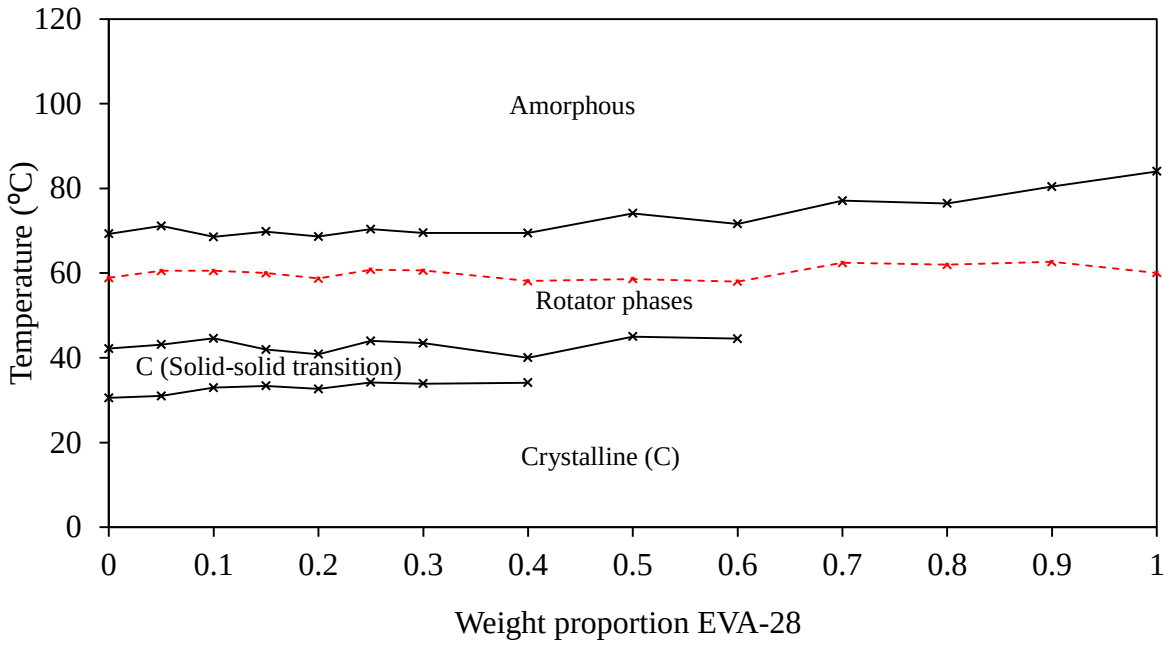

Figure 7: Blend melting phase diagram from DSC data. Lines from bottom to top illustrate; initiation of solid-solid transition, end point of solid-solid transition in the blends, peak melting point of the blends and point of complete blend melting.

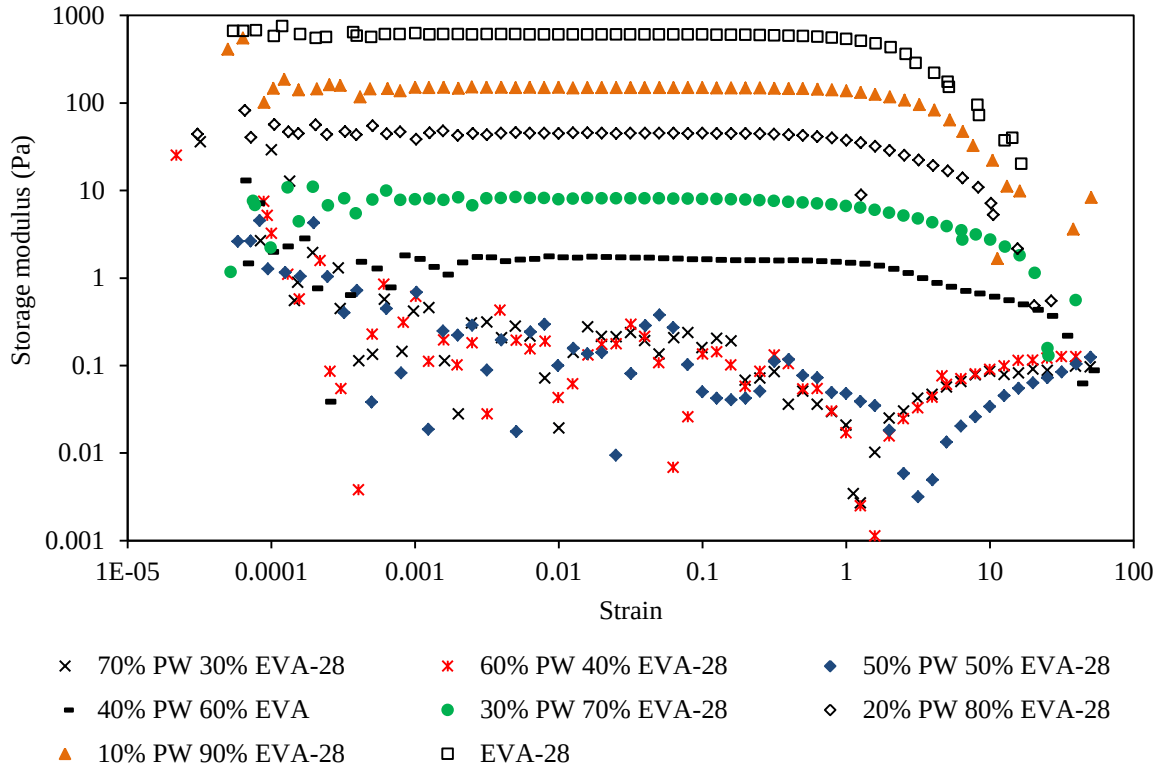

Figure 8: Strain sweep tests (at 1 Hz) for PW/EVA blends at 80 °C describing each blend's LVR.

Temperature sweeps can be observed for four selected blends in Figure 9, with all testing carried out in the pre-determined LVR. The congealing point is the cross-over point in the elastic (storage) and viscous modulus (45;46). The elastic modulus describes the solid element of the structure whereas the viscous modulus describes the liquid element of the blend with the point of cross-over highlighting the change in material behaviour from liquid-like dominance to that of solid-like dominance.

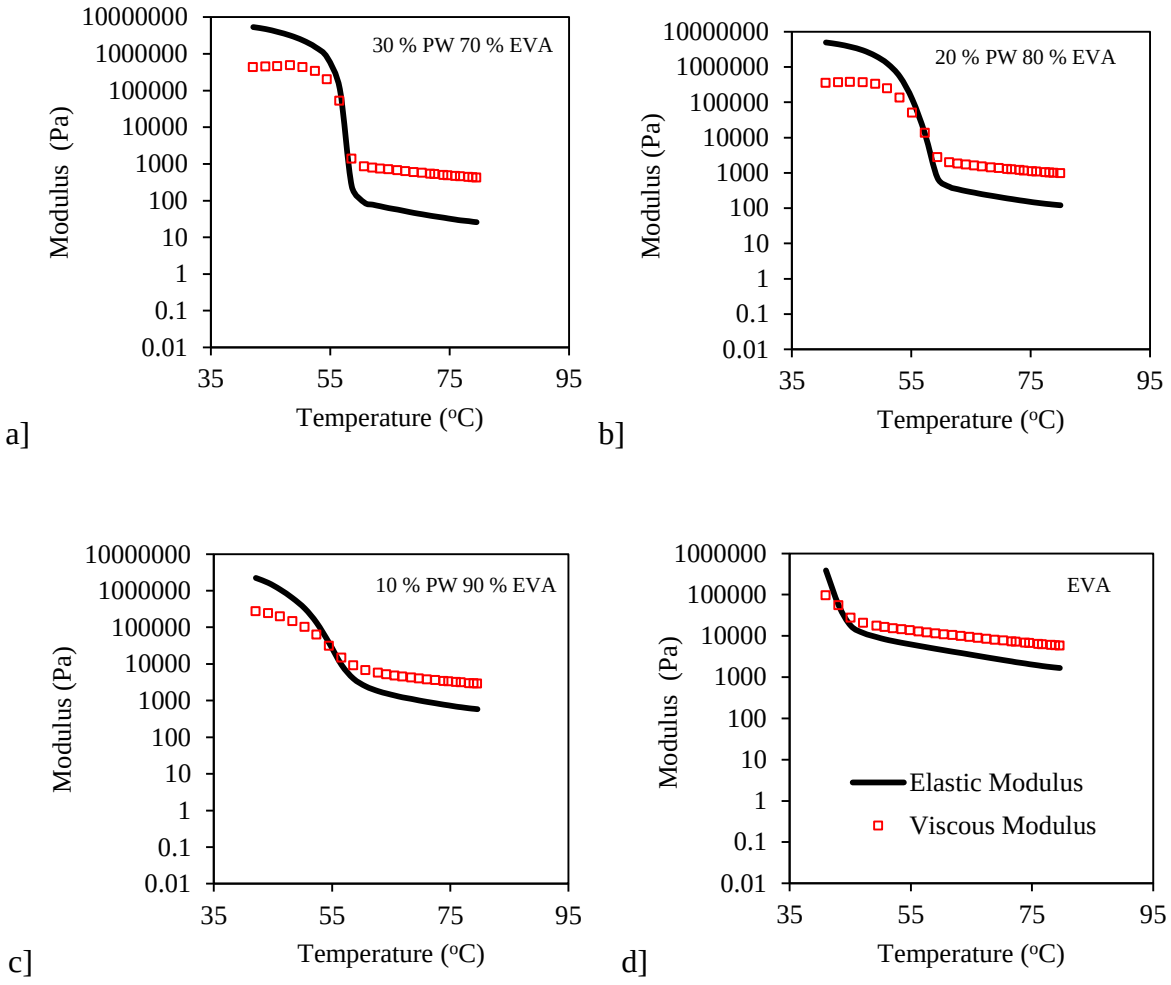

Figure 9: Temperature sweeps on selected PW/EVA blends in respective LVR's; a) 30 % PW 70 % EVA b) 20 % PW 80 % EVA c) 10 % PW 90 % EVA d) 100 % EVA.

The congealing point for all measurable blends is displayed in Figure 10 as a function of increasing EVA content. It should be noted that the congealing point of all formulated blends appears to coincide with the onset of solidification in PW as determined by DSC analysis, Figure 18. The weak structure of blends can also be highlighted through yield stress testing on the molten blends at 80 °C, shown in Figure 11, here yield stress is insignificant below forty weight percent of EVA. However, above that concentration of EVA and up to a 90 % addition there is a steady increase in the blend yield stress, before a sharp increase is observed between 90 and 100 %. The increased yield stress is thought to be due to the longer EVA molecules causing increasing interactions that require alignment before flow.

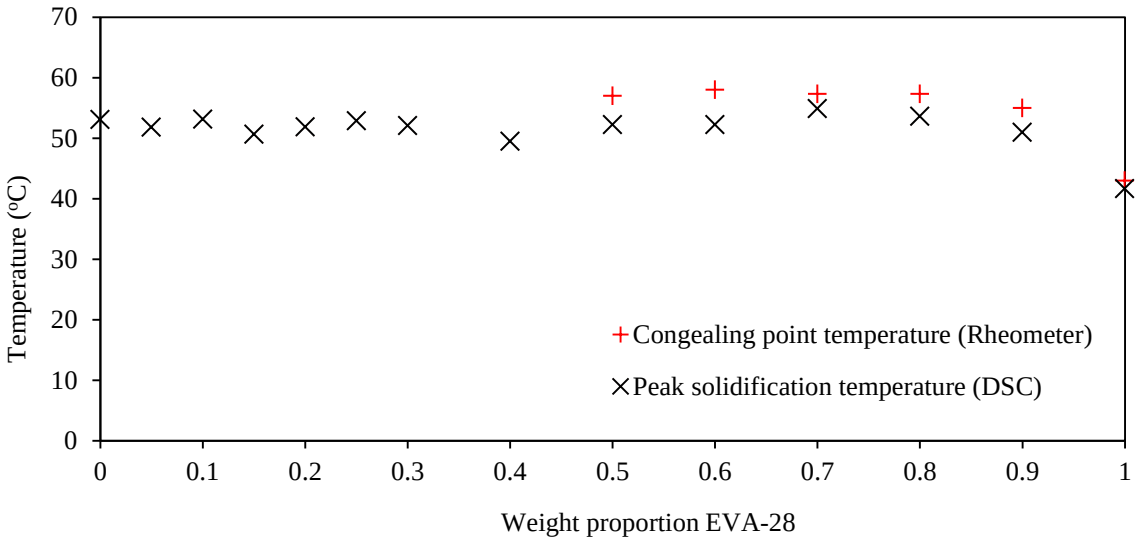

Figure 10: Comparison between congealing point and main solidification peak with EVA content.

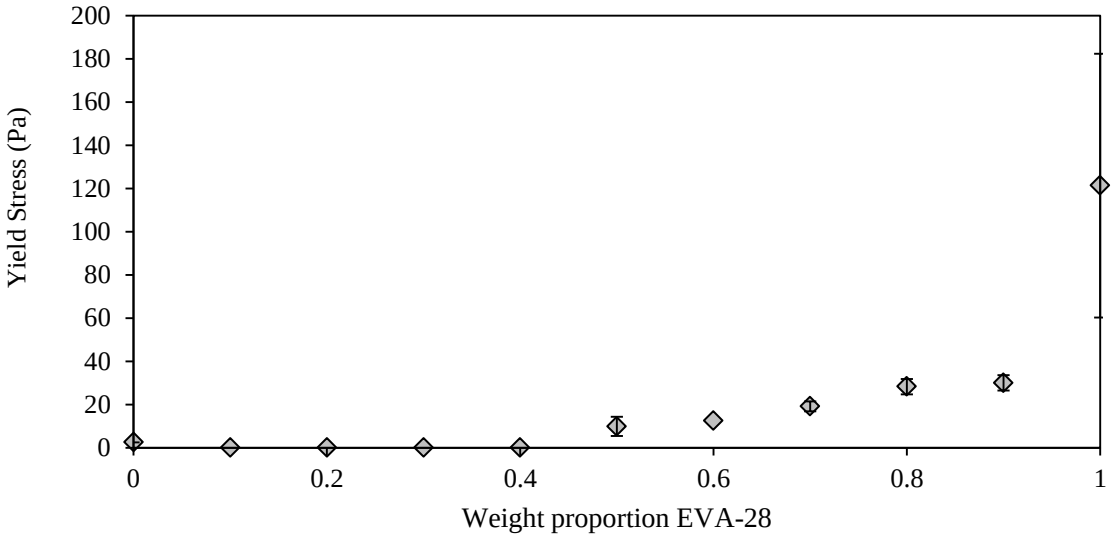

Figure 11: Yield stress of PW/EVA blends at 80 ^{o}C.

3.4 Flow Characteristics

3.41 Effect of Shear

Typically shear rates during injection moulding range between 100 s^{-1} to 1000 s^{-1} with the shear rate magnitude affecting materials to different extents. It is shown, Figure 12, that both Newtonian and shear thinning behaviour are exhibited by all the PW/EVA blends which is the desired characteristics needed for moulding applications as stated by Mutsuddy (2). All data sets with 30 % and greater EVA-28 content best fit to the Cross model, however, the Carreau model fits with similar success due to the models both being based on a low shear rate limiting viscosity and a high shear rate limiting viscosity which the blend tend towards (47) .

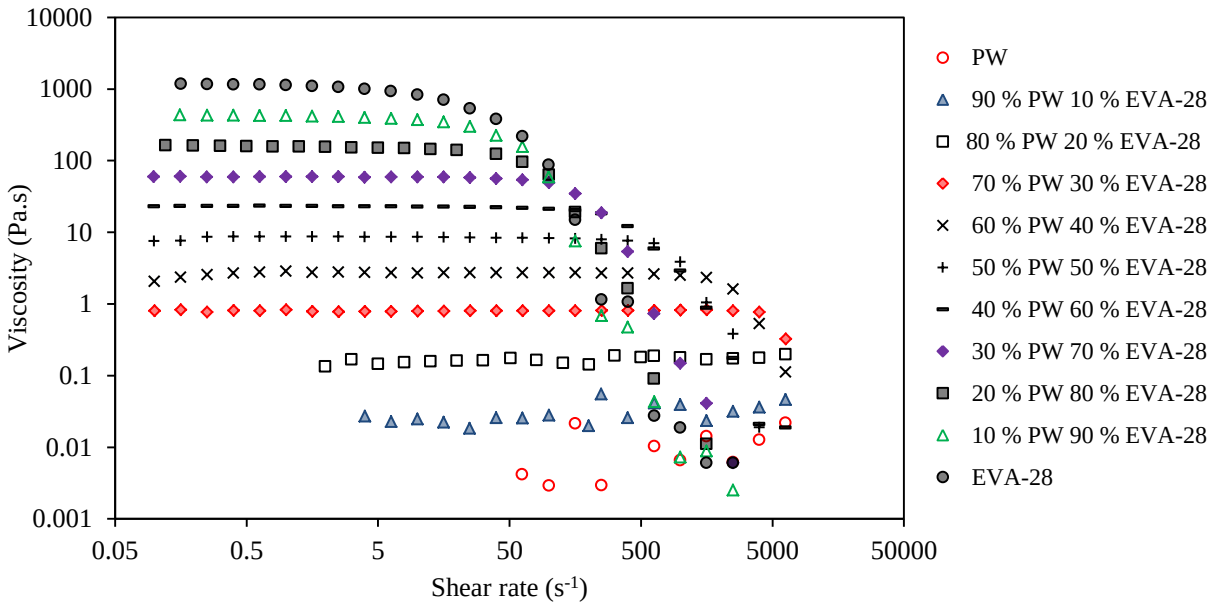

Figure 12: Effect of shear rate on the flow behaviour of PW and EVA blends at 80 ^{o}C.

PW does not appear to be stable under the experimental conditions due to the fluctuations observed in the measurements which is thought to be due to its low viscosity and weak bonding in its molten state coupled with rheometer capability, this is also proposed to be the case for the greater fluctuations seen in the blend with 10 % EVA.

With high concentrations of EVA in a blend (thirty weight percent and higher) the material exhibits a Newtonian behaviour at low shear followed by a shear thinning character at higher shear rates. This behaviour can be explained by the untangling and aligning of the long EVA chains at increased shear rates which subsequently reduces the flow resistance and hence viscosity. With low concentrations of EVA in a blend (less than thirty weight percent) a Newtonian behaviour is measured after initial viscosity equilibrium is met, which may be

explained by the limited long EVA chains present amongst the short chain length PW molecules allowing unrestricted movement at high shear.

In the typical injection moulding shear rate range, 100 to 1000 s^{-1}, formulated blends with thirty weight percent and less EVA maintain a Newtonian behaviour throughout, which may allow for greater control of paste during injection.

The onset of the shear thinning character in the blends with high EVA content differs with the proportion of EVA incorporated, Figure 13. It is proposed that, at higher concentrations of EVA, there is less free space for chain movement to occur before enforced alignment, and once alignment occurs a steep viscosity decrease is seen. On closer inspection of the data for blends containing between 50 and 100 weight percent EVA, it can be seen that shear thinning begins occurring at shear rates less than 100 s^{-1}. Blends with 100, 90 and 80 weight percent EVA appear to initiate shear thinning well below 100 s^{-1} whereas the blend with 70 weight percent EVA addition initiates thinning just above 100 s^{-1}. In these compositions a decay curve can accurately model the behaviour.

Potentially a shear thinning material could fill certain dies easier, however, it should be noted that the degree of shear a material undergoes in certain regions of dies during filling is likely to be low and so if shear thinning only initiates when subjected to large shear these benefits will be limited.

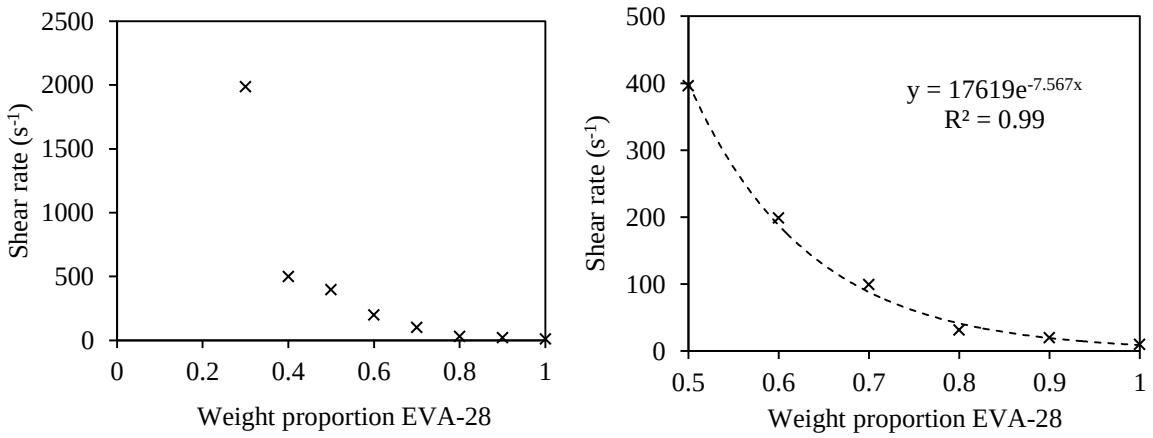

Figure 13: Magnitude of shear rate which initiates shear thinning behaviour in PW/EVA blends at 80 ^{o}C. The right hand graph expands the left hand graph for the region 50-100 weight percent EVA.

3.42 Effect of Temperature

The flow behaviour of the carrier vehicle melt has a strong bearing on the ability of the respective paste to fill a mould (47;48). Literature also states that for a carrier system a benchmark viscosity of less than 10 Pa.s at the moulding temperature when subjected to a shear rate of 100 s^{-1}, results in favourable outcomes (2). The implications of higher viscosity is more difficulty filling a component mould, which becomes more critical for complex

geometries. Higher pressures are also required to inject more viscous blends which will have financial implications and may detrimentally affect the binder properties.

The blends were cooled from 95 ^{o}C down to 40 ^{o}C, and the resultant rheological curves are shown in Figure 14. The behaviour can be split into three general stages, the first is a melt viscosity region from 95 ^{o}C to around 58-59 ^{o}C, which can modelled using the Arrhenius equation (47). This precedes a stage of significant viscosity increase brought on through the beginning of crystallisation / solidification in the blends. A final stage describes the interaction between the now solidified material under test and the geometry. This normally includes geometry slipping on the solidified material causing a lower than expected viscosity or geometry sticking on the solidified material causing a termination in the geometry movement before the final programmed temperature is met. Both forms of the third stage behaviour were observed for the PW/EVA blends.

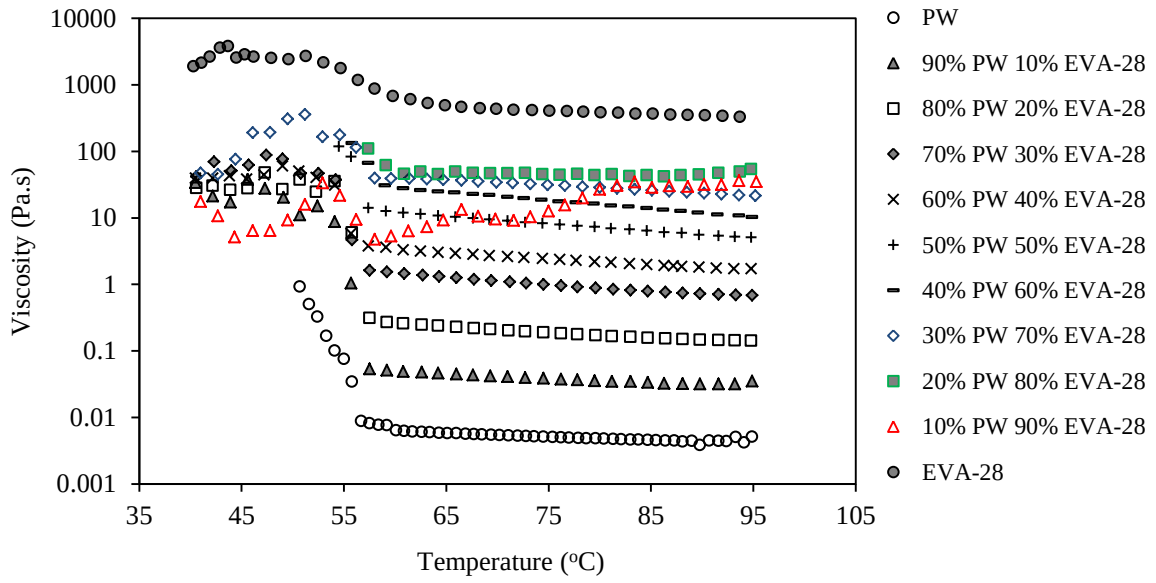

Figure 14: Flow behaviour of PW/EVA blends to changes in temperature (95-40 ^{o}C at a ramp of 10 ^{o}C.min^{-1} and a shear rate of 100 s^{-1} (blends are weight percent).

An increased proportion of EVA in a blend causes a corresponding increase in the melt viscosity, an observation attributed to the longer chains found in the EVA causing increasing interlinking, producing more resistance to flow. There is a general correlation between viscosity in the melt and the increasing EVA content up to a sixty weight percent addition of EVA, Figure 15.

Unusual relative flow behaviour occurs for blends with 70 to 90 weight percent EVA-28, which is thought to be due to the magnitude of the shear rate used during testing causing shear thinning in the material as supported in Figures 12 and 13. Once solidification takes place in these blends at lower temperatures there is still an observed increase in their blend viscosity due to the bulk solidification. EVA-28 appears to have shear thinning character initiated with low shear rates, Figure 13, however, it does not adversely affect its viscosity in

Figure 14 in line with the other blends. An explanation may be the fact EVA is a hot melt adhesive which may cause the material to physically attach to the measuring geometry and not 'thin' as would be expected (49;50).

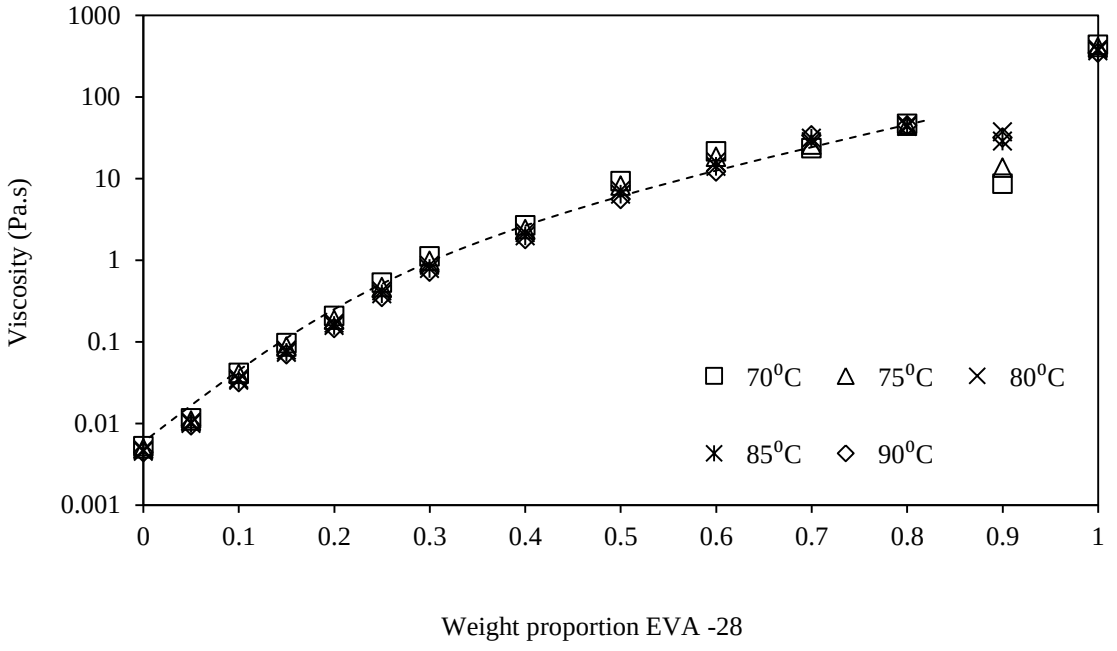

Figure 15: Effect of temperature on the melt viscosity of PW/EVA blends (shear rate 100 s^{-1}).

3.43 Blend Solidification

After successful injection and filling of the die, the feedstock cools and solidifies in the predetermined shape. Changes in properties of the carrier system during cooling, have a direct influence on how these steps should be conducted. Solidification from the melt has important implications to both the flow behaviour and the resultant mechanical strength of the PW/EVA blends, with each having a direct bearing on the flow of the paste formulated from them and mechanical properties of the moulded component respectively (51).

The solidification of PW and EVA are displayed in the DSC traces of Figure 16 and Figure 17 respectively. With PW, as temperature is reduced from the melt phase solidification eventually takes place which denotes the formation of the Rot. II phase. As temperature is reduced further different rotator phases may be present before the Rot. I phase is formed (34). With EVA a sharp peak is observed describing a fairly narrow chain length distribution for the polyethylene. This is a noticeable point of interest when comparing the difference in the melting and cooling DSC profiles for EVA, Figure 4 and Figure 17. On melting there is a broad peak and on cooling there is a sharp narrow peak, Kim states the differing behaviour between melting and solidification is due to the vinyl acetate forming none-crystallisable intra-molecular defects that contribute to a wide size distribution of crystallites that require different amounts of energy to melt (52). The exothermic DSC traces in Figure 18 describe the effect of cooling the PW/EVA blends, with the profiles highlighting the formation of crystal elements as energy is released.

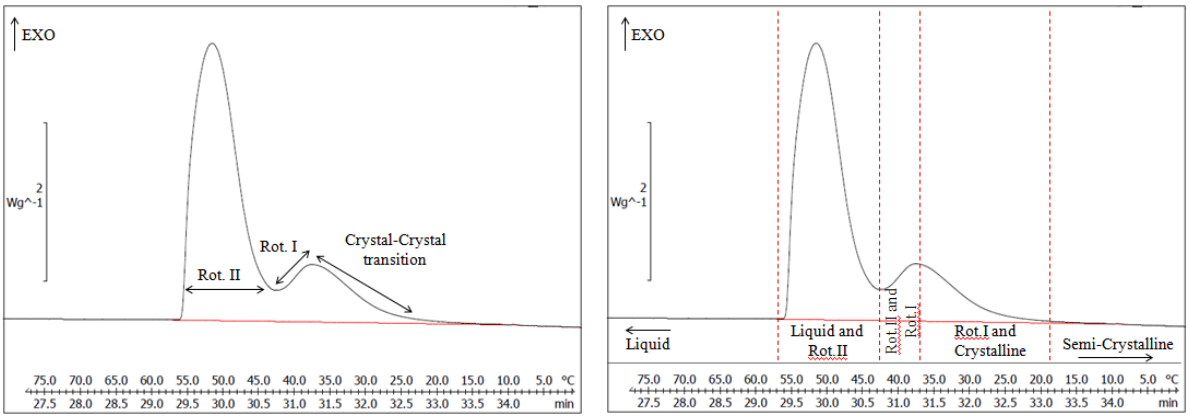

Figure 16; DSC cooling trace of paraffin wax (ramp rate of 10 $^{o}C{\cdot}min^{-1}$) describing transitions (left) and state of material (right) with decreasing temperature.

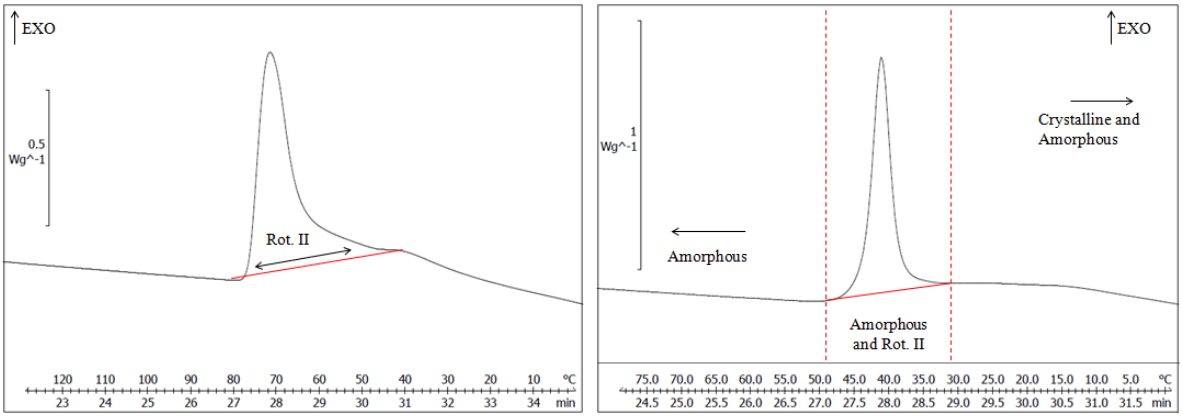

Figure 17; DSC cooling trace of EVA (ramp rate of 10 $^{o}C{\cdot}min^{-1}$) describing transitions (left) and state of material (right) with decreasing temperature.

The transition points from cooling cycle 1 are plotted in Figure 19 with Figure 20 illustrating the proposed transitions occurring in two selected blends, 70 % PW 30 % EVA and 30 % PW 70 % EVA. The solidification onset temperature for all blends is mostly unchanged with EVA additions, appearing to highlight that PW dominates the solidification kinetics due to it solidifying at higher temperatures compared to the crystalline polyethylene segments in EVA. It is also observed that the crystals start forming at lower temperatures than the melting temperature of them and this is a well-documented occurrence due to the temperature driving force required to allow crystal nucleation and growth to occur (53).

The crystal-crystal, Rot. I and Rot. II transitions formed in PW are also unchanged up to a forty weight percent addition of EVA. As EVA additions are increased further it appears that the Rot. I phase is no longer formed, however, it is stated in literature that the Rot. I phase can be depressed in mixtures (34). At high EVA contents it appears that there is a direct transition from the Rot. II phase to the crystalline phase during cooling.

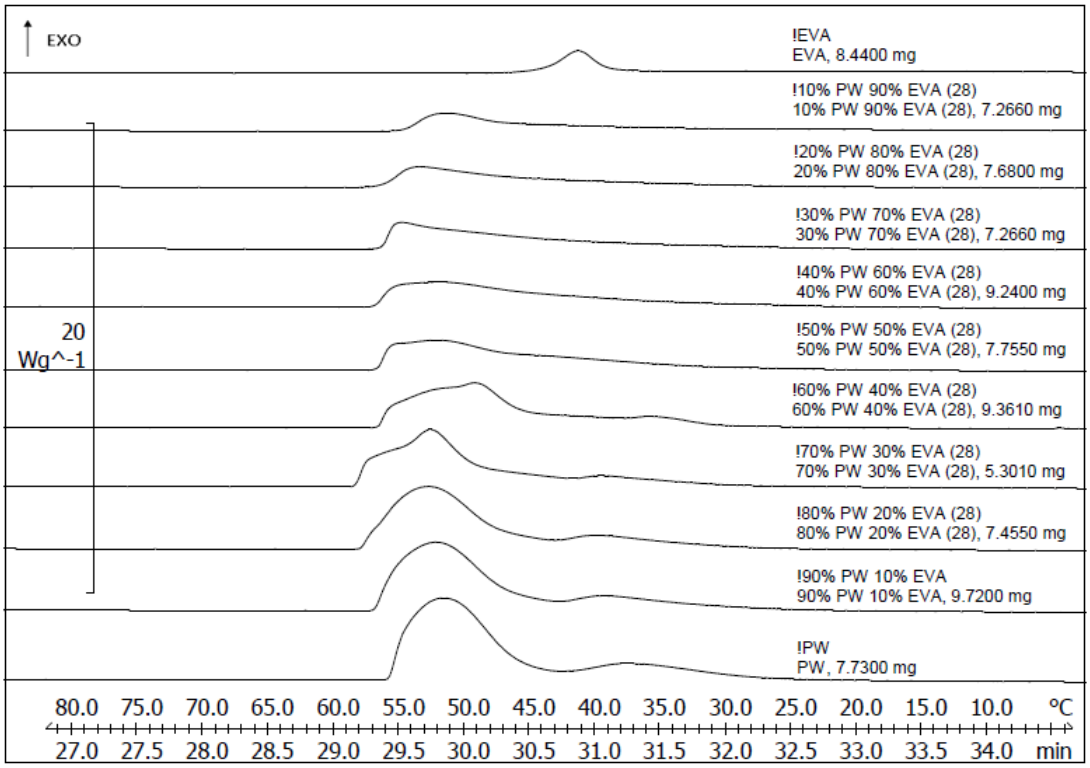

Figure 18: DSC analysis of paraffin wax and ethylene vinyl acetate blends (Cooling cycle 1 from 150 °C to -20°C at 10 °C·min^{-1}).

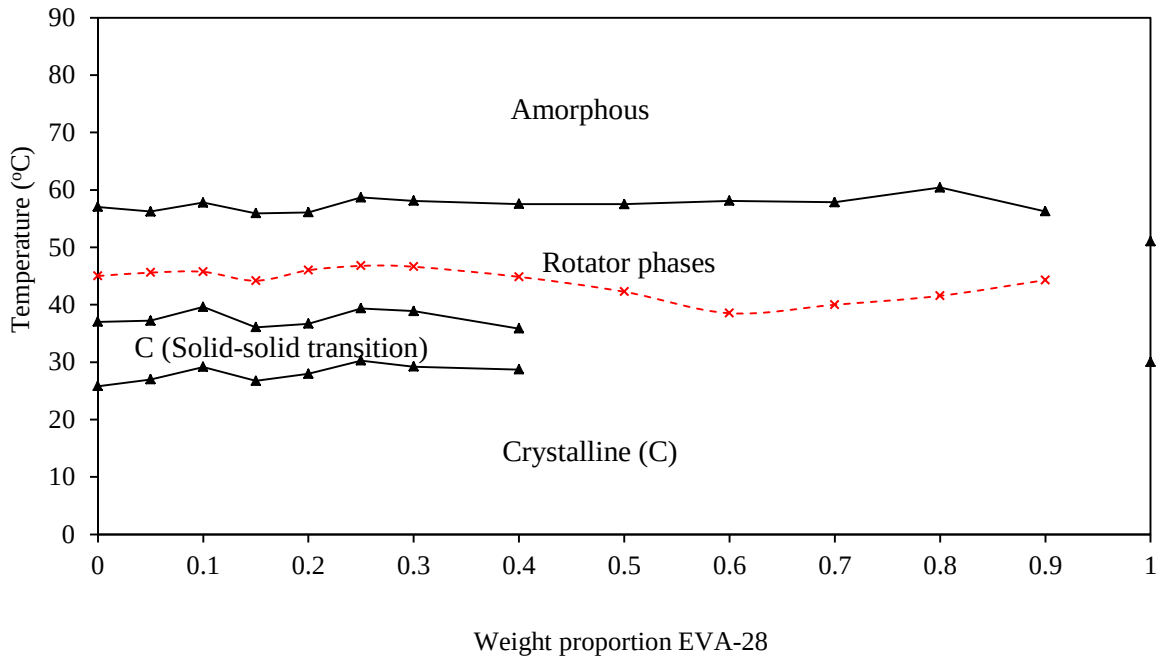

Figure 19: PW/EVA blend solidification phase diagram from DSC data. Lines from top to bottom illustrate; onset of solidification, peak solidification point of the blends, initiation of the solid-solid transition and end point of solid-solid transition in the blends.

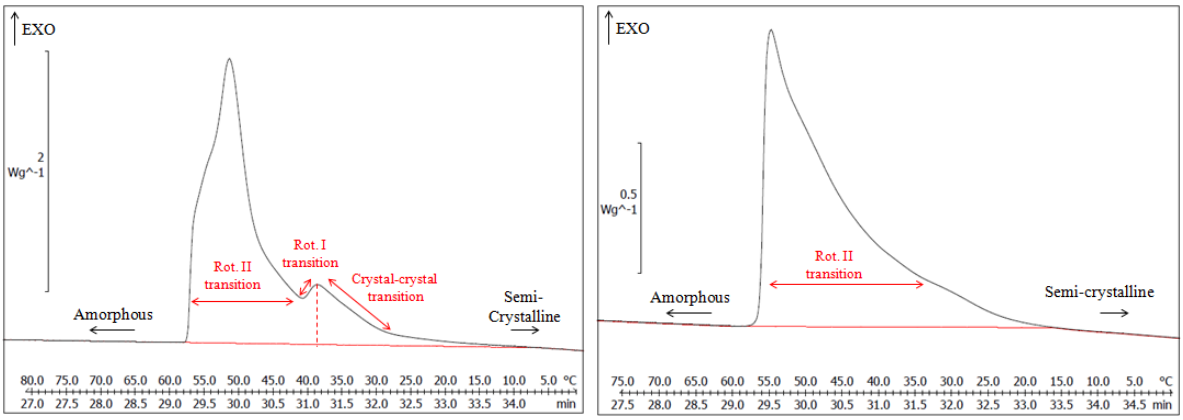

Figure 20; DSC cooling traces (ramp rate of 10 $^{o}C.min^{-1}$) for 70 % PW 30 % EVA (left) and 30 % PW 70 % EVA (right).

3.45 Blend Crystallinity

The crystallinity of the blends was determined using Equation 5 (22);

$$X_c^{DSC} = \frac{\Delta H_f}{\Delta H_m(1-\phi)} \qquad (5)$$

here ΔH_f is the heat of fusion/crystallisation obtained by integrating the area under the DSC traces, with ΔH_m being the enthalpy of a 100 % crystalline sample. ϕ is the weight fraction of each material in the blend.

There appears to be a strong negative correlation (R^2 value of 0.99) between increasing EVA content and decreasing crystallinity in the formulated blends, Figure 21. This correlation is consistent for both the melting and cooling profiles. This leads to the conclusion that there is little to no interactions between the materials in the blends and the strong correlation also implies the formulations are well mixed. Figure 22 highlights how total crystallinity is split between PW and EVA in the blends as the EVA content is increased.

3.46 Mechanical Strength

A carrier vehicle requires a degree of flexural strength to aid in the reduction of defects formed during component cooling in the die, as well as the handling defects caused by component movement when in the green state. It is known that mechanical properties of the moulded green core is directly related to those of the carrier vehicle (51). Representative profiles of each blend from three point flexural testing are displayed in Figure 23.

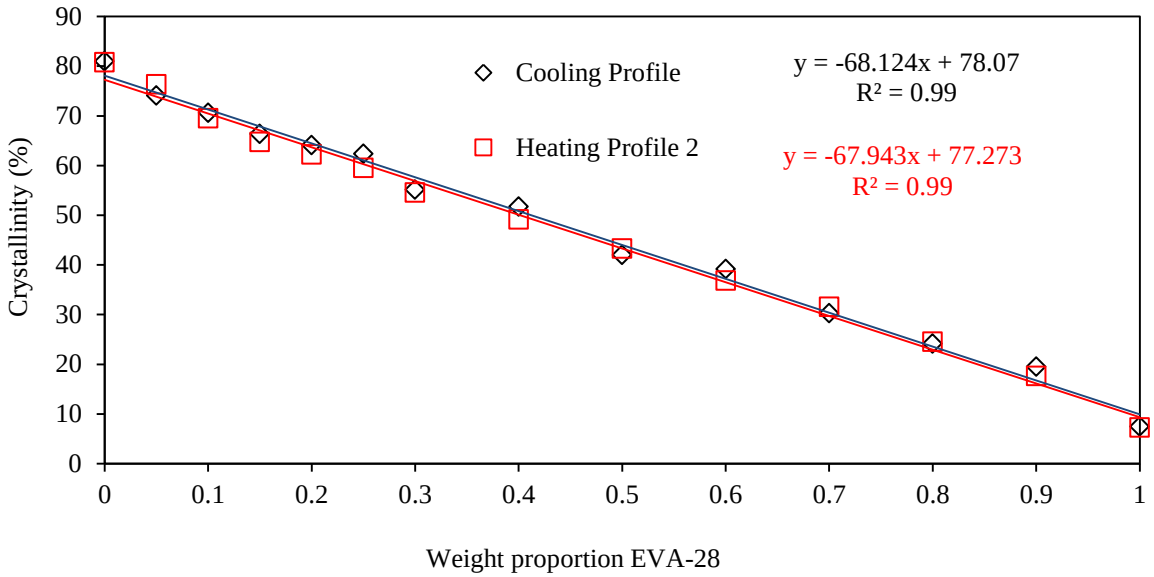

Figure 21: Crystallinity of PW/EVA blends (for both heating and cooling).

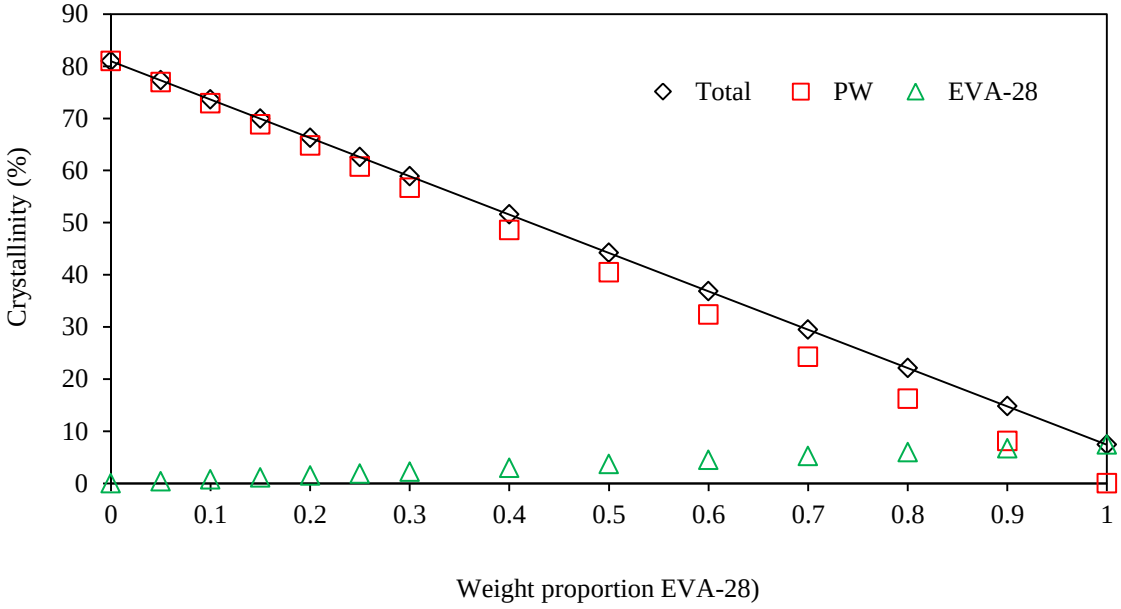

Figure 22: Crystallinity of PW/EVA blends (cooling profile) describing how total crystallinity is split between material types.

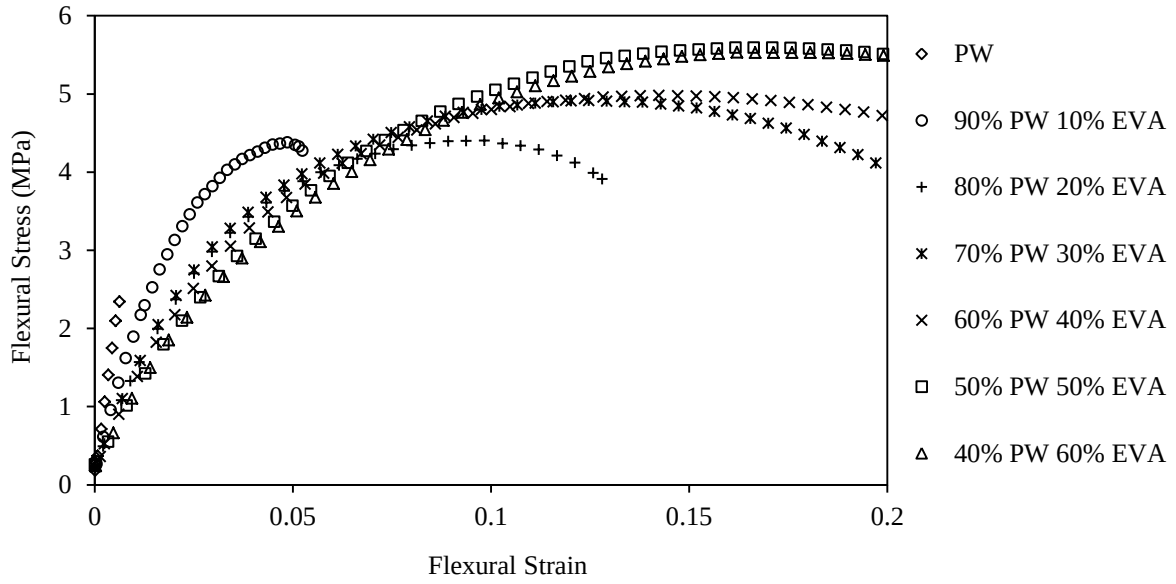

Figure 23: Flexural behaviour profiles of PW/EVA blends (displaying representative profiles).

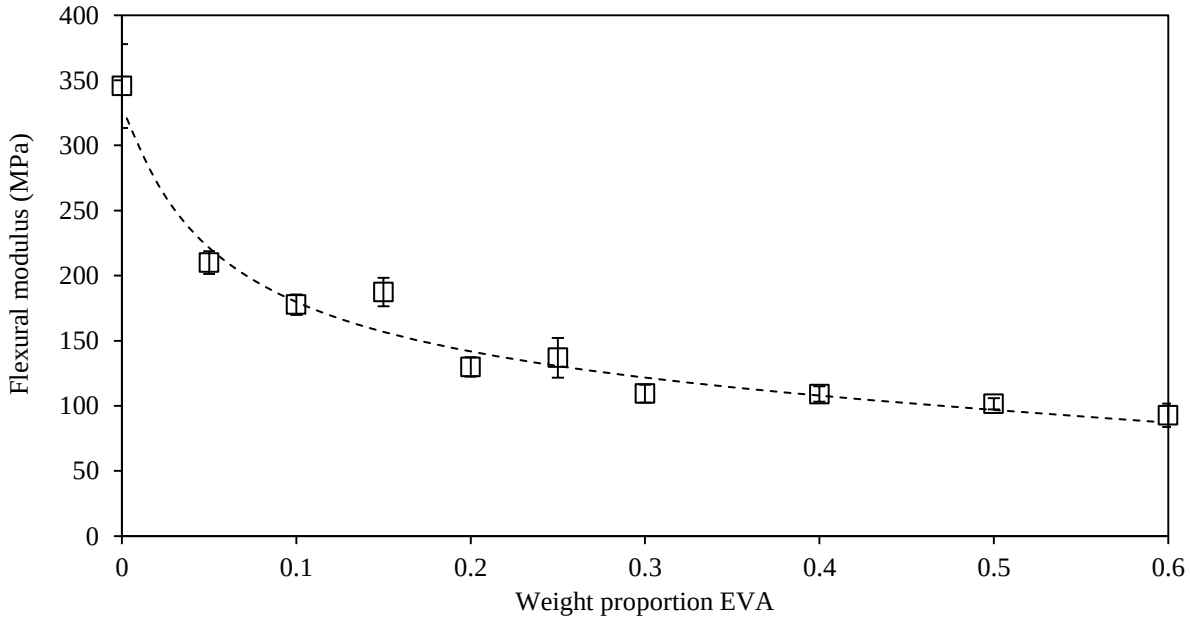

Figure 24: Flexural modulus of the PW/EVA blends.

With increasing EVA content there is an observed trend of decreasing flexural modulus, highlighted more clearly in Figure 24 describing the blends becoming progressively less stiff with more EVA. A behaviour which is believed to be due to the long EVA chains forming an interconnecting network in the structure giving the blends more plastic properties. The maximum flexural stress and strain achieved for each blend is numerically illustrated in Figure 25, with the low variance between the blends suggesting consistent structure formation. There is a trend of increasing maximum flexural strength and strain achieved at this stress, highlighting an increased elastic character and greater flexibility.

PW has a low flexural strength (a factor of the load at failure) and experiences brittle failure at small flexural strains due to the easy propagation of cracks through its crystalline structure. With only a five weight percent addition of EVA to PW the flexural strength of the resultant blend approximately doubles, it is proposed this is due to the crack propagation being retarded by the long EVA chains within the PW matrix. Further additions of EVA, up to twenty-five weight percent, cause only marginal increases in the flexural strength. It is proposed that this marginal increase is because the EVA chains are already interlinked throughout the whole material, but do slightly increase the resistance to crack propagation. Here the network structure is sufficient to inhibit pure brittle failure but insufficiently developed to give purely plastic deformation.

The ability of blends to restrict crack propagation is further illustrated with the increased strain attained at maximum stress with greater EVA content, a strong correlation (0.996) is reported. Energy to fracture information also illustrates this correlation between increasing EVA content in a blend and increased resistance to crack propagation, Figure 26.

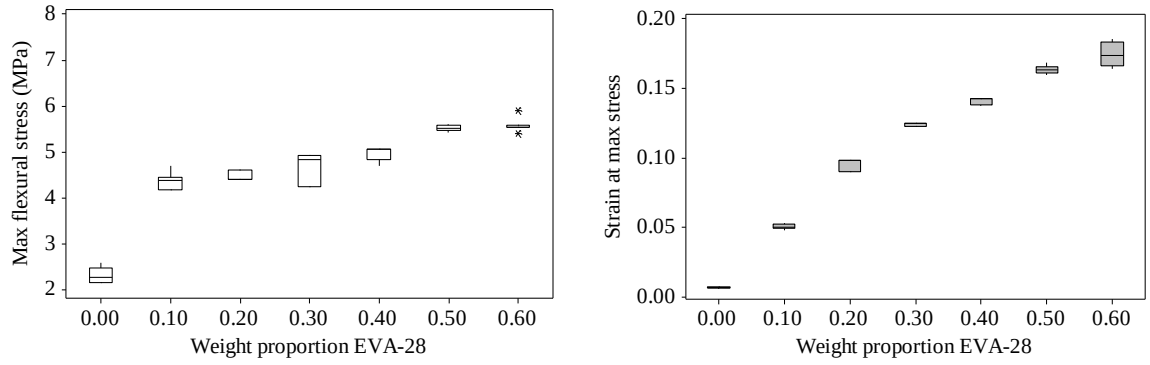

Figure 25: Behaviour of PW and EVA blends to an applied load.

The solidification process has been captured by hot stage optical microscopy (HSOM), Figure 27. The crystallisation of PW illustrates needle type crystals forming from the melt at approximately 57 ^{o}C (54). The crystalline features occur at random nucleation points, highlighting slight impurities, and grow from these points as the temperature decreases. Focus is lost at lower temperatures due to the cumulative growth of polycrystals and due to the short depth of field of the microscope.

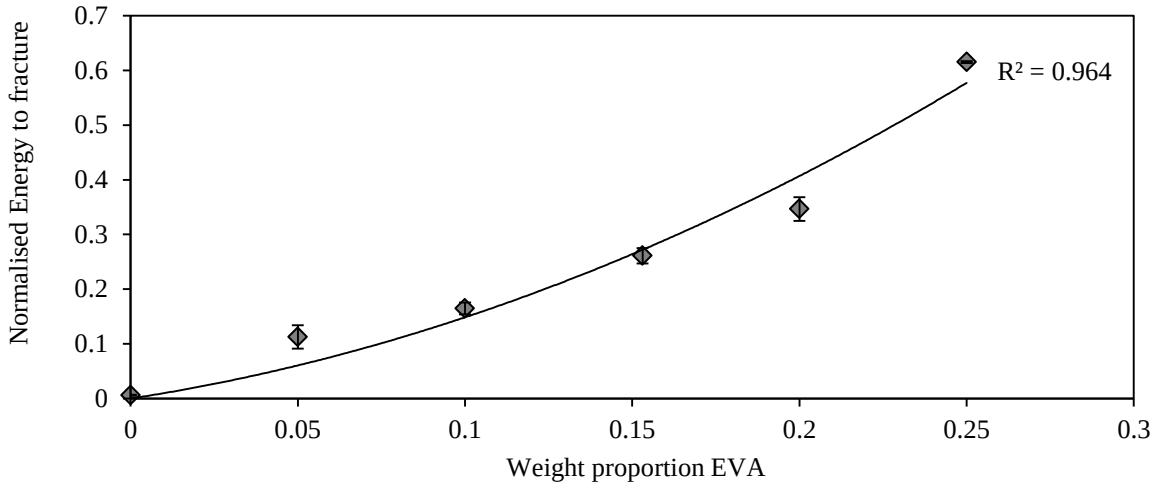

Figure 26: Energy to fracture of PW/EVA blends.

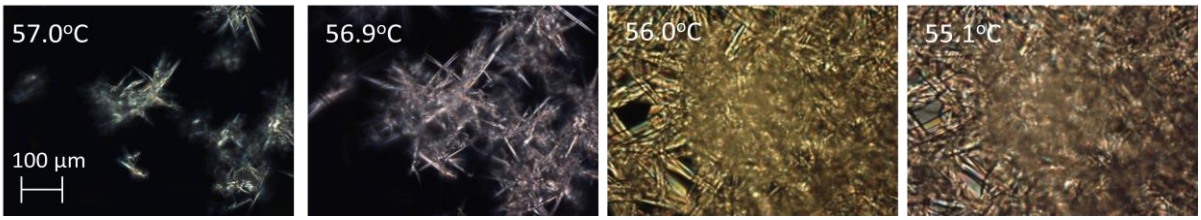

Figure 27: Solidification of paraffin wax (Cooling rate of 1 $^{o}C{\cdot}min^{-1}$).

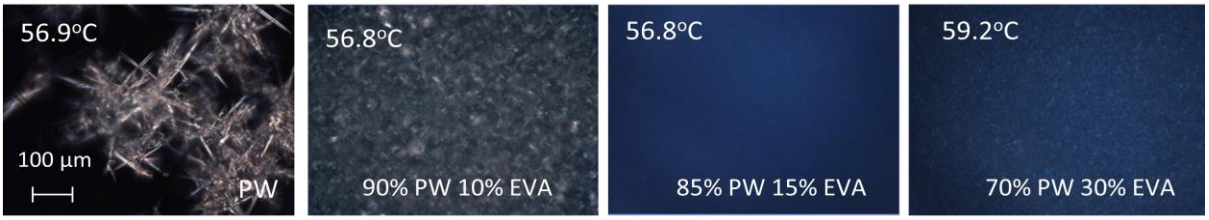

Figure 28: Effect of EVA content on crystalline formation in PW/ EVA blends (Cooling rate of 1 $^{o}C{\cdot}min^{-1}$).

There is a marked difference in crystalline formation, Figure 28, when EVA is added to PW with the drop in the crystalline artefact size clearly observed, a factor also observed in the literature (20). Unfortunately when the EVA content is increased crystal formation becomes difficult to observe which is due to the ever decreasing crystal fraction in the amorphous matrix. Although difficult to observe it is possible to see crystalline elements spread throughout the amorphous material when 30 % EVA is added.

From the microscopy images it can be observed that the crystalline forms appears to get smaller with EVA additions, thought to be a result of growth suppression by the increasing amorphous material content, thus making the material more resistant to crack propagation. The more developed the amorphous matrix the greater the energy required for cracks to propagate through the entirety of the material.

4. Conclusions

The thermal behaviour of PW/EVA blends will strongly influence the required processing conditions for CIM. On melting increasing the EVA content in blends causes a subsequent increase in the blend melting point. However, on cooling the low crystallinity in EVA-28 means the congealing point of each blend is almost identical to the peak solidification temperature of PW.

PW/EVA blends experience shear thinning behaviour with increasing shear rate, which can be modelled with reasonable accuracy using the Cross model although the Carreau model describes similar behaviour. An increase in the EVA content causes shear thinning to initiate at lower shear rate values, but also forms a blend with an increasing elastic character in the melt. Using a carrier system viscosity guideline developed by Mutsuddy, viscosity at injection should be ideally less than 10 Pa.s when exposed to a shear rate of 100 s^{-1} suggesting the maximum content of EVA-28 for a successful paste is in the region of 50 weight percent.

Increasing the additions of EVA to PW retards brittle fracture in the resultant material and acts to develop an increasing degree of plastic deformation before fracture. Failure is even prevented at concentrations over 25 weight percent. The increase in EVA content in blends also acts to reduce their flexural modulus.

5. Reference List

(1) Z.Y.Lui, N.H.Loh, S.B.Tor, K.A.Khor, Y.Murakushi, R.Maeda. Binder System for Micropowder Injection Moulding. Materials Letters 2001;(48):31-8.

(2) B.C.Mutsuddy and R.G.Ford. Ceramic Injection Moulding. Chapman and Hall; 1995.

(3) B.Loebbecke, R.Knitter, J.Hausselt. Rheological properties of alumina feedstocks for the low-pressure injection moulding process. Journal of the European Ceramic Society 2009;29(9):1595-602.

(4) S.Blackburn and D.I.Wilson. Shaping ceramics by plastic processing. Journal of the European Ceramic Society 2008;28:1341-51.

(5) A.Dakskobler, T.Kosmac. Rheological properties of re-melted paraffin-wax suspensions used for LPIM. Journal of the European Ceramic Society 2009;29:1831-6.

(6) W.Yang, K.Yang, M.Hon. Effects of PEG molecular weights on the rheological behavior of alumina injection molding feedstocks. Materials Chemistry and Physics 2002;78:416-24.

(7) P.Thomas-Vienna, B.Levenfeld, A.Varez, A.Cervera. Production of Alumina parts by powder injection moldingwith a binder system based on high density polyethylene. Journal of the European Ceramic Society 2008;(28):763-71.

(8) C.Hsu, J.Lee, K.Jaw. Decompositon of binder from a ceramic injection molding sample. Thermochimica Acta 2000;367-8.

(9) M.T.Zaky, F.S.Solimon, A.S.Farag. Influence of paraffin wax characteristics on the formulation of wax-based binders and their debinding from green molded parts using two comparative techniques. Journal of Materials processing Technology 2009;(209):5981-9.

(10) T.Jardiel, M.E.Sotomayor, B.Levenfeld, A.Varez. Optimization of the Processing of 8-YSZ Powder by Powder Injection Molding for SOFC Electrolytes. International Journal of Applied Ceramic Technology 2008;5(6):574-81.

(11) G.Bandyopadhyay, K.W.French. Injection-molded Ceramics: Critical Aspects of the Binder Removal Process and Component Fabrication. Journal of the European Ceramic Society 1993;11:23-34.

(12) M.Trunec and J.Cihlar. Thermal removal of multicomponent binder from ceramic injection mouldings. Journal of the European Ceramic Society 2002;(22):2231-41.

(13) D.Lui, W.J.Tseng. Rheology of injection-molded zirconia-wax mixtures. Journal of materials science 2000;35:1009-26.

(14) R.Wu, W.Wei. Torque evolution and effects on alumina feedstocks prepared by various kneading sequences. Journal of European ceramic society 2000;20:67-75.

(15) S.W.Kim, H.Lee, H.Song. Effect of minor binder on capillary structure evolution during wicking. Ceramics International 1999;25:671-6.

(16) S.Ren, X.He, X.Qu, I.S.Humail, Y.Wei. Influence of binder composition on the rheological behaviour of injection-molded microsized SiC suspensions. Journal of University of Science and Technology Beijing 2010;15(3):297-301.

(17) O.Bemblage, D.B.Karunakar. A Study on the blended wax patterns in investment casting process. 2011 p. 1-7.

(18) M.Attarian, E.Taheri-Nassaj, P.Davami. Effect of ethylene-vinyl acetate copolymer on the rheological behaviour of alumino-silicate/polyethylene wax suspension. Ceramics International 2002;28:507-14.

(19) H.S.Ashbaugh, X.Guo, D.Schwahn, R.K.Prud'homme, D.Richter, L.J.Fetters. Interaction of paraffin wax gels with ethylene/vinyl acetate co-polymers. Energy and Fuels 2005;19:138-44.

(20) E.Marie, Y.Chevalier, F.Eydoux, L.Germanaud, P.Flores. Control of n-alkanes crystallisation by ethylene-vinyl acetate copolymers. Journal of colloid and interfacial science 2005;290:406-18.

(21) M.Song, M.Park, J.Kim, I.Cho, K.Kim, H.Sung, et al. Water-soluble binder with high flexural modulus for powder injection moulding. Journal of Material Science 2005;40:1105-9.

(22) X.M.Shi, J.Zhang, J.Jin, S.J.Chen. Non-isothermal crystallisation and melting of ethylene-vinyl-acetate copolymers with different vinyl acetate contents. eXPRESS Polymer Letters 2008;2(9):623-9.

(23) N.Ukrainczyk, S.Kurajica, J.Sipusic. Thermophysical Comparison of Five Commercial Paraffin Waxes as Latent Heat Storage Materials. Chemical and Biochemical Engineering Quarterly 2010;24(2):129-37.

(24) S.Ghose, K.A.Watson, D.C.Working, J.W.Connell, J.G.Smith Jr, Y.P.Sun. Thermal conductivity of ethylene vinyl acetate copolymer/nanofiller blends. Composites Science and Technology 2008;68(7-8):1843-53.

(25) P.Mullinger, B.Jenkins. Industrial and Process Furnaces - Principles, Design and Operation. Elsevier; 2008.

(26) G.Wypych. Handbook of Fillers. 3 ed. ChemTec Publishing; 2010.

(27) T.R.Crompton. Thermo-oxidatative degradation of polymers. Smithers Rapra Technology; 2010.

(28) Rubber Nanocomposites - Preparation, properties and Applications. John Wiley & Sons; 2010.

(29) I.RAy, S.Roy, T.K.Chaki, D.Khastgin. Studies of thermal degradation behaviour of EVA/LDPE blend. Journal of Elasomers and Polymers 1994;26:168.

(30) E.B.Sirota, H.E.King J, D.M.Singer, H.H.Shao. Rotator phases of the normal alkanes: An x-ray scattering study. The Journal of Chemical Physics 1993;98(7):5809-24.

(31) J.Wang, S.J.Severtson, P.H.Geil. Brittle-ductile transitions and the toughening mechanism in paraffin/organo-clay nanocomposites. Materials Science and Engineering A 2007;467:172-80.

(32) M.Dirand, M.Bouroukba, V.Chevallier, D.Petitjean. Normal alkanes, multialkane synthetic model mixtures, and real petroleum waxes: Crystallographic structures,

thermodynamic properties, and crystallization. Journal of Chemical Engineering Data 2002;47(2):115-43.

(33) X.Guo, B.A.Pethica, J.S.Huang, R.K.Prud'homme. Crystallization of long-chain n-paraffins from solutions and melts as observed by differential scanning calorimetry. Macromolecules 2004;37:5638-45.

(34) E.B.Sirota, H.E.King J, G.J.Hughes, W.K.Wan. Novel Phase Behavior in Normal Alkanes. Physical Review Letters 1992;68(4):492-5.

(35) N.Jung, M.Yun, S.Joen. Phase Transitions between the rotator phases of paraffin investigated using silicon microcantilevers. The Journal of Chemical Physics 2012;136-40.

(36) I.I.Gnatyuk, N.V.Platonova, G.A.Puchkovskaya, E.N.Kotelnikova, S.K.Filatov, J.Baran, et al. Polymorphic Transformations of C26H54 and C28H58 n-Paraffins as Typical Rotator Substances. Journal of Structural Chemistry 2007;48(4):654-65.

(37) E.B.Sirota, H.E.King J, H.H.Shao, D.M.Singer. Rotator Phases in Mixtures of n-Alkanes. Journal of Physical Chemistry 1995;99:798-804.

(38) S.J.Severtson, M.J.Nowak. Molecular Restructuring Kinetics and Low-Velocity Wetting of n-Alkane Rotator Phases by Polar Liquids. Langmuir 2002;18:9371-6.

(39) O.Shobanjo. Fundamental study of the waxes used in investment casting [Eng-D thesis] University of Birmingham; 2010.

(40) M.Dirand, M.Bouroukba, A.Briard, V.Chevallier, D.Petitjean. Temperatures and enthalpies of (solid + solid) and (solid + liquid) transitions of n-alkanes. J Chem Thermodynamics 2002;34:1255-77.

(41) G.Meyer, M.Matthai, J.Auge, H.Lindow. Crystallisation Processes and Hardness of Paraffin Waxes Characterised by DSC, Ultrasonic, X-Ray and Needle Penetration Measurements. SOFW-Journal 2005;(131):3-9.

(42) K.Agroui, G.Collins, J.Farenc. Measurement of glass transition temperature of crosslinked EVA encapsulant by thermal analysis for photovoltaic application. Renewable Energy 2012;43:218-23.

(43) Y.Shieh, Y.Lin. Induced crystallisation of EVA having various VA contents by compressed CO2. Journal of Applied Polymer Science 2002;87(7):1144-51.

(44) T.S.Piwonka, K.A.Woodbury, J.M.Wiest. Modelling casting dimensions: Effect of wax rheology and interfacil heat transfer. Materials and Design 2000;21:365-72.

(45) A.M.Rao. Rheology of Fluid and Semisolid Foods - Principles and Applications. Springer-Verlag; 1999.

(46) C.Fuentes-Auden, F.J.Martinez-Boza, F.J.Navarro, P.Partal, C.Gallegos. Formulation of new synthetic binders: Thermo-mechanical properties of recycled polymer/oil blends. Polymer Testing 2007;26:323-32.

(47) C.K.Schoff and P.Kamarchik. Rheology and rheological Measurements. 2005.

(48) S.K.Samanta, H.Chattopadhyay, M.M.Godkhindi. Thermo-physical characterisation of binder and feedstock for single and multiphase flow of PIM 316L feedstock. Journal of Materials processing Technology 2011;211:2114-22.

(49) Y.Park, H.Kim. Hot-melt adhesive properties of EVA/aromatic hydrocarbon resin blend. International journal of adhesion and adhesives 2003;23:383-92.

(50) Y.Park, H.Joo, H.Do, H.Kim. Viscoelastic and adhesion properties of EVA/tackifier/wax ternary blend systems as hot-melt adhesives. Journal of adhesion science technology 2006;20(14):1561-71.

(51) J.Kim, B.Kim. Effect of the Liquid-Liquid Phase Separation on the Crystallization Behaviour and Mechanical Properties of Poly(ethylene-ran-vinyl acetate) and Paraffin Wax Blend. Journal of Polymer Science 1999;37:1991-2005.

(52) N.Somrang, M.Nithitanakul, B.P.Grady, P.Supaphol. Non-Isothermal melt crystallization kinetics for ethylene-acrylic acid copolymers and ethylene-methyl acrylate-arylic acid terpolymers. European Polymer Journal 2004;40:829-38.

(53) A.G.F.Stapley, H.Tewkesbury, P.J.Fryer. The effects of shear and temperature history on the crystallisation of chocolate. Journal of the American Oil Chemists' Society 2007;76:677-85.

(54) R.T.Edwards. Crystal Habit of Paraffin Wax. Industrial and Engineering Chemistry 1957;49(4):750-7.